

Time-Resolved Brain-to-Heart Probabilistic Information Transfer Estimation Using Inhomogeneous Point-Process Models

Vincenzo Catrambone , Alireza Talebi, Riccardo Barbieri , Senior Member, IEEE, and Gaetano Valenza , Senior Member, IEEE

I. INTRODUCTION

Abstract—Objective: The quantification of functional brain–heart interplay through the dynamics of the central and autonomic nervous systems may provide effective biomarkers for cognitive, emotional, and autonomic state changes. Despite several computational models were proposed to this end, none provides a directional estimation of such interplay in a time-resolved and probabilistic fashion. **Methods:** In this study, a multivariate inhomogeneous point-process model for heartbeat dynamics is employed to derive subject-specific, time-resolved, functional estimates of the directional interplay occurring from the brain to the heart, whose activity is represented by electroencephalography and R-peaks intervals series. An inverse-Gaussian probability density function is used to predict heartbeat events as a function of neural dynamics, which is modeled as an exogenous input to the autoregressive cardiac dynamics. **Results:** The performance is evaluated using heart rate variability and electroencephalography series gathered from 24 healthy volunteers undergoing a cold-pressor test, and the modeling goodness-of-fit is assessed through the time-rescaling theorem. The results suggest that cortical dynamics drives heartbeat series with specific time delays in the range of 30s to 60s and 90s to 120s from the peripheral thermal stress onset. **Conclusion:** The proposed framework provides novel insights in human neurophysiology, exploiting a fully probabilistic definition of the continuous functional brain–heart interplay.

Index Terms—Electrocardiography, electroencephalography, brain modeling, physiology.

Manuscript received January 20, 2021; revised March 29, 2021; accepted March 31, 2021. Date of publication April 6, 2021; date of current version October 20, 2021. This work was supported in part by the European Commission H2020 Framework Programme under Grant 101017727 of the Project EXPERIENCE, and in part by the Italian Ministry of Education and Research (MIUR) in the framework of the “Department of Excellence” CrossLab Project. (Corresponding author: Vincenzo Catrambone.)

Vincenzo Catrambone is with the Department of Information Engineering and Bioengineering and the Robotics Research Center E. Piaggio, School of Engineering, University of Pisa, 56126 Pisa, Italy (e-mail: vincenzo.catrambone@ing.unipi.it).

Alireza Talebi and Gaetano Valenza are with the Department of Information Engineering and Bioengineering and the Robotics Research Center E. Piaggio, School of Engineering, University of Pisa, Italy.

Riccardo Barbieri is with the Department of Electronics, Informatics, and Bioengineering, Politecnico di Milano, Italy.

This article has supplementary downloadable material available at <https://doi.org/10.1109/TBME.2021.3071348>, provided by the authors.

Digital Object Identifier 10.1109/TBME.2021.3071348

KNOWLEDGE of functional brain–body interplay is important because of the strong physiological and clinical reciprocal implications that exist between central and peripheral systems. Consequently, the discovering of the brain–heart interplay dynamics could yield insights regarding the joint activity, in physiologic and pathological conditions, of the autonomic nervous system (ANS) and the central nervous system (CNS).

Such an interaction has been mainly formalized with the definition of the central autonomic network (CAN) [1]–[5], which includes brain regions involved in the control of the ANS, such as circulatory and autonomic regulation. It has been reported that the amygdala, the anterior cingulate cortex, the anterior insula, the hypothalamus, the parabrachial nuclei, periaqueductal grey matter, and some medulla areas are involved in cardiac function modulation, and all belong to the CAN [6]. The CAN organization reveals how cognitive and mental processes can trigger autonomic responses and bodily arousal [7] and, consequently, any injury, dysfunction, or certainly a stroke, localized in these brain areas may strongly affect cardiovascular functions.

The nucleus of the tractus solitarius, located in the medulla, is a relay center, connected to the dorsal motor nucleus of the vagus nerve. The latter directly controls activation of the parasympathetic nerves innervating the cardiac system, while the sympathetic outflow is governed by the paraventricular nucleus, the rostral ventro-lateral medulla, and the rostral ventromedial medulla [5], [8]. Contrary to the sympathetic nerves having direct influence on heart period shortening, the activity of the parasympathetic nerves increases the heart period [5].

Many neurological, psychiatric, and cardiovascular disorders may be related to CAN dysfunctions. Exemplarily, cerebrovascular accidents and transient ischaemic attacks are frequently caused by cardiac arrhythmias [9], while atrial fibrillation may result in cognitive disorders [10], [11]. Moreover, severe head injuries or stroke affecting cortical and subcortical areas such as medial prefrontal cortex and insula may lead to cardiac arrhythmias [12], in particular sinus tachycardia, hyper/hypo-tension, or sudden cardiac death [5]. Recent studies have reported a significant correlation between mental disorders and cardiovascular dysfunctions, for example, mental stress and bipolar disorders with ischemia and chronic disease [13]–[16].

ANS control of the heart as measured through Heart Rate Variability is related to attentional regulation, affective information processing, physiological flexibility, and cerebral blood flow [1], [17]–[21]. Distinct patterns of ANS responses are witnessed in the expression of emotions (e.g., [22]) for which a visceral homunculus may exist [23]. Dysfunctions of the ANS were found in acute and chronic stressful conditions [12], insomnia [24], psychosomatic disorders [25] and schizophrenia, anxiety and mood disorders (e.g., [26], [27]), while somatic consequences in depression are also thought to be due to metabolic, immunoinflammatory, and autonomic dysregulations [28].

It is therefore evident that proper methodology to quantify the functional brain–heart interplay may be crucial for the objective diagnosis and treatment monitoring of CAN-related diseases.

There have been a number of studies that have attempted to uncover functional brain–heart interplay in different conditions, some of them mainly focused on the characterization of the phenomenon as a black box, while others have tried to mathematically model it. One may account for the study of neural events that occur concurrently to heartbeats; while the basic idea follows the rationale behind event-related potential analysis and heartbeat-evoked potential [29], a functional brain–heart co-occurrence analysis may be extended beyond second-order statistics, i.e., in the multifractal domain [30].

Other functional brain–heart interplay estimation methods rely on information-theoretic metrics applied to brain- and heartbeat-derived time series, such as the maximal information coefficient [31], [32], transfer entropy [33], convergent cross-mapping [34], and joint symbolic analysis [35].

Furthermore, the so-called “network physiology” approach identifies brain–heart interplay as a part of a broader network in which other physiological systems are involved (e.g., respiration), and all possible pairwise interactions are measured [33], [36]. Multivariate models for electroencephalographic (EEG) and R-R intervals series have also been proposed to estimate functional brain–heart interplay by exploiting Granger causality [37], [38], as well as ad-hoc synthetic data generative models [39].

Until recently, the proposed models for studying brain–heart interplay have encountered major limitations, among which that the phenomenon is not addressed in a probabilistic fashion, and without the model’s goodness-of-fit metrics. Of note, state-of-the-art modeling for functional brain–heart interplay assessment has not provided effective time-resolved estimates. Indeed, EEG dynamics might be much faster than cardiovascular dynamics, and the sampling times are often very different. Thus, to have insight into the continuous cortical regulation of cardiovascular function, it might be important to find a methodology that addresses the coupling between EEG rhythms and heart function (heartbeat).

In the present work, we propose a novel probabilistic framework for functional brain–heart interplay assessment whose theoretical foundations lie in inhomogeneous point-process theory and transfer entropy estimation, and preliminary results were reported in [40]. The time series given by the instants of R-peak events from the electrocardiogram is a well-known

non-stationary and complex signal [41]. Hence, the signal interpolation is not such an accurate technique of signal preparation for further analysis, e.g., the Fourier transform. For this reason, we employed inhomogeneous point-process modeling, which goes beyond interpolation [42]. The point-process model considers human heartbeats or R-peak events, which are discrete in time, and attempts to provide a continuous-time representation for human heartbeat based on firing time distribution of the sinoatrial node, modeled as an inverse-Gaussian model. The inverse-Gaussian model parameters, which are employed in the Z-transform to study heartbeat dynamics in the frequency domain, are instantaneously updated. The probabilistic nature of the model provides the model goodness assessment via strong tools, such as the Kolmogorov–Smirnov (K-S) plot, and the autocorrelation function.

When considering the brain-to-heart functional direction, the model is able to provide time-varying estimates within a fully probabilistic framework along with goodness-of-fit metrics. This model is mathematically defined in the continuous time domain to derive the information transfer from EEG to heartbeat dynamics at each moment in time. Specifically, the directional, functional brain–heart interplay quantification from the brain to the heart is achievable through the definition of transfer entropy between the two systems. More details on model parametrization and goodness-of-fit evaluation are available in [42], [43], and in section II of this paper. The proposed model is able to estimate the probability of heartbeat occurrence based on the history of the process, including the past R-peak events (heartbeats) and the EEG power spectral density (PSD) in the frequency bands representative of cortical involvement (i.e., δ , θ , α , β , and γ).

To validate the model, we exploited a dataset, previously employed in [39], comprising R-R intervals and EEG series recorded from 24 healthy subjects under the cold-pressor test (CPT), which is a strong thermal stress leading to a notable sympatho-vagal elicitation. CPT triggers physiological mechanisms, such as baroreflex, through increased sympathetic activity of the ANS to maintain the body homeostatic condition [44]. The CPT is a widely used test for the study of autonomic functions of the body [45]–[49], as well as the study of CNS reaction to strong temperature and sub-threshold painful stimuli [50]–[52].

Neuroimaging studies highlighted that brain correlates of CPT involve several CAN areas [53]–[56]. Cortical correlates of CPT include frontal areas in the δ [50], [51], and θ frequency bands [50], posterior-parietal areas in the α band [50], [51], and peripheral bilateral temporal regions in the β band [50]. Beyond linear spectral analysis, in a previous study we found that the cortical response to CPT involves responses in the multifractal domain, particularly in the prefrontal, left-temporal, and right-posterior parietal areas [52]. In summary, two clusters in fronto-temporal and posterior-parietal areas are involved in the neuro-physiological response to CPT, along with the significant autonomic - sympathovagal - response. Importantly, functional brain–heart interplay correlates of CPT involve a brainstem activation. In fact, all afferent signaling involving peripheral receptors and effectors rely on brainstem nuclei, including the

synthesis and release of specific neurotransmitters and neuro-modulators for autonomic control [57], [58].

II. MATERIALS AND METHODS

A. Point-Process Theory for Cardiovascular Dynamics

Considering R-peaks within electrocardiogram recording as representative of human heartbeat dynamics, the resulting R-wave events sequence expresses a discrete representation for human heartbeat in which the interval between two consecutive points is called the R-R interval. The point-process modeling of this phenomenon provides a continuous representation of human heartbeat based on the probability function of the waiting time for the next heartbeat. This probability function is obtained as a history-dependent inverse-Gaussian distribution function as follows [42], [59]:

$$f(t) = \left(\frac{\kappa}{2\pi(t - u_k)^3} \right)^{1/2} \exp \left(-\frac{\kappa[t - u_k - \mu]^2}{2\mu^2(t - u_k)} \right) \quad (1)$$

where u_k is the most recent (k^{th}) R-wave event before time t ; $\kappa > 0$ and μ are a shape parameter and the instantaneous mean value, respectively. It is possible to define $N(t) = \max\{k : u_k \leq t\}$ as the sample path of the related counting process. Its differential, $dN(t)$, denotes a continuous-time indicator function: $dN(t) = 1$ when there is an event, otherwise it is null. The left continuous sample path is defined as $\tilde{N}(t) = N(t^-) = \max\{k : u_k \leq t\} = j$. The instantaneous mean value is defined by taking recent R-R intervals as the history of heartbeat dynamics using an autoregressive model as follows [42]:

$$\mu_{RR}(t) = a_0 + \sum_{i=1}^p a_i RR_{\tilde{N}-i} \quad (2)$$

where RR_i is the i^{th} R-R interval; p is the model order; and $a = (a_0, \dots, a_p)$ are the model parameters estimated by the local maximum likelihood method. The model goodness-of-fit is assessed by applying the time-rescaling theorem on inhomogeneous Poisson rates calculated by the conditional intensity function via Eq. (1) [42], [43].

B. Bivariate Point Process Model of Brain–Heart Interplay

We next explain a new time-varying model of the brain–heart interplay based on the point-process modeling framework addressed in the previous session. Employing a bivariate model, the cortical involvement in cardiovascular regulation through the sino-atrial node is an exogenous input assigned to the simple autoregressive model from Eq. (2). The new model is defined as follows:

$$\mu_{\phi-RR}(t) = a_0 + \sum_{i=1}^p a_i RR_{\tilde{N}-i} + \sum_{j=1}^q b_j \phi_{\tilde{N}-j} \quad (3)$$

where RR_i is the i^{th} RR interval, similar to Eq. (2); ϕ_j is the time-varying EEG dynamics; a_i and b_j are the model coefficients; and p and q are the model orders. In this study, ϕ_j is the PSD of a single EEG channel in a given EEG band.

The coefficient weighting the exogenous input to the autoregressive model describes the functional brain–heart interplay. Furthermore, by substituting Eq. (3) into Eq. (1), all parameters can be estimated by the local maximum likelihood method [42], [60], and the model goodness-of-fit is assessed as in the previous section. The estimated parameters are time-resolved and estimated every 5ms [42], [60], and the modeling is fully probabilistic with evaluable goodness-of-fit.

Instead of using common methods of model selection, such as the Akaike information criterion, we select the optimal model orders $\{p, q\}$ using an iterative approach in accordance with the K-S test and related statistics [42], [60]. With this concept, the optimal model order is selected when the cumulative distribution function lies on the diagonal line (the cumulative distribution function of a perfect uniform distribution) between two confidence bounds. In this study, p and q are set to 9 and 5, respectively.

C. Time-Resolved Transfer Entropy

Transfer entropy is a non-parametric measure of information transfer among distinct systems [61]. It determines whether information of the linked system X to the system Y is useful for estimating the events of the system Y . Having the probability functions of two process X and Y , we have:

$$TE_{X \rightarrow Y}(t) = E \left\{ \log \frac{f_{Y(t)|H_{Y(t)}, H_{X(t)}}(y(t)|H_{Y(t)}, H_{X(t)})}{f_{Y(t)|H_{Y(t)}}(y(t)|H_{Y(t)})} \right\} \quad (4)$$

where $H_{X(t)}$ and $H_{Y(t)}$ are histories of X and Y processes. Referring to Eqs. (2) and (3), and having the probability distribution function of the process $R - R$ derived from Eq. (1), the information transfer from the EEG to the heartbeat is defined as follows [60]:

$$TE_{EEG \rightarrow RR}(t) = E \left\{ \log \frac{f_{RR(t)|H_{RR(t)}, H_{\phi(t)}}(RR(t)|H_{RR(t)}, H_{\phi(t)})}{f_{RR(t)|H_{RR(t)}}(RR(t)|H_{RR(t)})} \right\} \quad (5)$$

Eqs. (2) and (3) provide us with an explicit definition of inverse-Gaussian probability density functions of heartbeat dynamics in the continuous time. Considering the brain and the heart as two systems for which we are interested in measuring information transfer, the associated point-process transfer entropy from the EEG to the R-R intervals series is defined as follows [60]:

$$I_{B \rightarrow H}(t) = E \left\{ \log \frac{f_{t|H_{RR(t)}, H_{\phi(t)}}(t|H_{RR(t)}, H_{\phi(t)})}{f_{t|H_{RR(t)}}(t|H_{RR(t)})} \right\} \quad (6)$$

where $I_{B \rightarrow H}(t)$ defines the directional information transfer from the EEG to the R-R intervals series. This formulation provides a quantitative measure of functional brain–heart interplay.

Eq. (6) may be explicated to its closed form based on the estimated model parameters and the Kullback–Leibler divergence for inverse-Gaussian probability density functions:

$$I_{B \rightarrow H}(t) = \frac{1}{2} \left[\ln \left(\frac{\kappa^{EEG-RR}}{\kappa^{RR}} \right) + \frac{\kappa^{RR}}{\kappa^{EEG-RR}} + \frac{\kappa^{RR} (\mu^{EEG-RR} - \mu^{RR})^2}{\mu^{RR} \mu^{EEG-RR}} - 1 \right] \quad (7)$$

where κ^{EEG-RR} and μ^{EEG-RR} are the model parameters from Eqs. (1) and (3); κ^{RR} and μ^{RR} are similar parameters coming from a univariate heartbeat model (see Eq. (2)) as in [60].

D. Experimental Data and Signal Preprocessing

The dataset employed in this study, already utilized in [39], has been collected from 30 healthy right-handed subjects (26.7 years on average; 15 males) who volunteered to participate in the study. Sitting comfortably on a chair, after 3 min of resting state, participants were asked to submerge their left (not-dominant) hand into iced water (below 4°) and maintain it in this position for up to 3 min. The choice of this timeframe was in accordance with the literature on pain perception [45]. Subjects were free to remove their hand if feeling uncomfortable or pain, and in fact six subjects were discarded for this reason. The experimental protocol had received approval by the local ethical committee Area Vasta Nord-Ovest Toscana. A 1-lead ECG, abdominal, respiratory activity and 128-channel EEG were simultaneously recorded during the experiment with a 500Hz sampling rate. Artifact free and of consistent CPT duration from 24 subjects were retained for further analyses.

The R-peak detection from the electrocardiogram signal was performed using the Pan-Tompkins algorithm [62]. Possible artifacts in the ECG signal are when a previous T-peak might be detected as the next R-peak (the weakness of the Pan-Tompkins algorithm for peak detection), inappropriate fixation of electrodes, and motion artifacts. These artifacts can be detected by looking at the R-R intervals series where several abnormal spikes are present. An online error detection and correction analysis pipeline performing point-process statistics including log-likelihood prediction was implemented on the RR-series, which helped avoid possible physiological (e.g., ectopic beats) or algorithmic (e.g., peak mis-detection) artifacts [63]. Finally, the processed segments were visually inspected before enrollment for further analyses.

EEG series were cleaned from noises and artifacts using EEGLAB [64] and HAPPE software, described in [65]. In brief, 90 channels were selected, the raw EEG signals were filtered through high-pass (1Hz cutoff) and low-pass (100Hz cutoff) filters. The 50-Hz power supply noise was removed using the multi-taper regression approach [65]. Bad channels were removed after identification with an electrode impedance check. HAPPE employs a powerful wavelet-enhanced independent component analysis, which removes several artifacts, such as eye blinks [65]. The remaining artifacts were removed by automated independent component analysis [65]. Finally, we

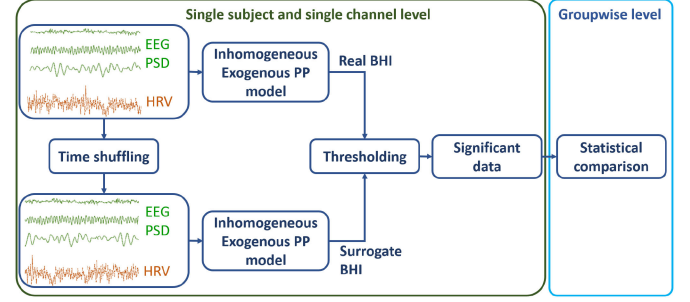


Fig. 1. Schematic representation of the analysis pipeline with the assessment of statistical significance.

performed bad-channel rejection and re-referencing of the EEG signals to their time-varying average.

The PSD of the signals was estimated using the averaged periodogram (Welch method) in each of five EEG frequency ranges: $\delta = [1, 4)$, $\theta = [4, 8)$, $\alpha = [8, 12)$, $\beta = [12, 31)$, and $\gamma = [31, 100]$ Hz, with 500 samples per window (1s duration), and 75% overlap.

Finally, the calculated EEG power was interpolated according to the R-event time instants to attain the same sampling frequency with the RR event series. Noted that the first 60s of the R-R intervals series is neglected due to the point-process algorithm, since this segment is considered for prediction of model parameters in the next 5ms. In fact, the 60-s window is shifted for 5ms and the new parameters are calculated until the end of the signal. The brain-to-heart interplay model is run for each channel/subject pair. Additionally, to have a consistent timeline among all subjects, we selected the first 120s of CPT.

E. Statistical Analysis

The reliability of functional brain–heart interplay estimates from the proposed framework were statistically evaluated through testing based on a surrogate data analysis under the null hypothesis of absence of causal interactions [66]. Briefly, synthetic data with the same distribution of the original time series and different autocorrelation function were generated by randomly permute the original samples. This shuffling should be performed independently for R-R intervals and EEG-PSD series.

For each subject recording, for each EEG electrode and frequency band, 50 random permutations of the original EEG-derived PSD time series (i.e., ϕ_j in Equation (3)) were generated, together with 50 random permutations of the original R-R intervals time series. The synthetic series were then used to get time-varying brain-to-heart estimates from the proposed methodology, and the distribution of these estimates would then constitute the null distribution in the uncoupling case. If the original brain-to-heart estimate is higher than the 90th percentile of the null distribution, then the estimate is reliable and may be retained for further analysis. Such a statistical assessment was repeated for all subject recordings and all EEG channels. A summary scheme of the analysis pipeline is depicted in Figure 1.

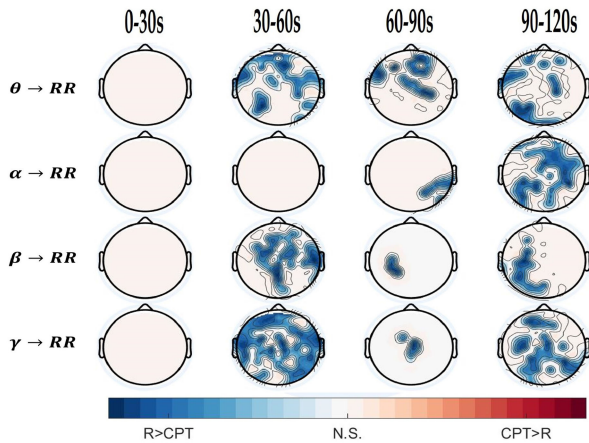


Fig. 2. The p-value topographic maps of $I_{B \rightarrow H}$ from rest vs. CPT statistical comparison resulting from the Wilcoxon test for the following pairs: rest vs. CPT [0,30]s, [30,60]s, [60-90]s, and [90 120]s. Red color highlights regions in which CPT has higher brain–heart interplay than rest, blue color means the opposite, whereas green color stands for not significant (N.S.) regions.

Reliable brain–heart interplay estimates were exploited to investigate significant changes between the resting state and the CPT session. To this end, CPT sections were divided into four equal non-overlapping segments (30s for each frame), and the statistical analysis was then performed. To compare different phases, we used the non parametric Wilcoxon signed-rank test for paired samples, which is robust against outliers and does not depend on the shape of the original distribution. Significance was chosen at 5%, and p-value correction for multiple comparison was performed through a permutation test with 1000 permutations. A spatial cluster-mass permutation correction was applied to assess the physiological plausibility of the results. We have two sets of p-values resulting from the Wilcoxon tests:

- (1) *Comparison between resting state and each 30s of CPT phase*: in this test, for each subject, we derived the median value of the brain-to-heart index during the resting state. We repeated the same procedure with the four non-overlapping time windows from the CPT phase. The Wilcoxon test was run, for each electrode, considering the median index extracted during resting state and each 30s window (Fig. 2).
- (2) *Comparison between resting state and CPT phase*: despite the previous test, we considered the whole CPT phase (2min) instead of segmenting it (Fig. 4).

Furthermore, we performed group-wise analyses to compare all experimental sessions - resting state and the four 30s windows of CPT - at once using the non-parametric Friedman test for paired samples.

All the results are plotted as topographic distributions of significant p-values from the associated tests, and topographic distributions of the statistics associated to the test. The group-wise median values for estimates from all experimental sessions can be found in the electronic Supplementary Material.

TABLE I
NUMBER OF SUBJECTS WHOSE $I_{B \rightarrow H}(t)$ ESTIMATES PASSED THE SURROGATE SIGNIFICANCE ANALYSIS FOR THE TWO EXPERIMENTAL CONDITIONS

Frequency band	Rest	CPT
δ	15	14
θ	17	14
α	16	14
β	19	14
γ	19	15

III. RESULTS

Table I shows the number of subjects whose $I_{B \rightarrow H}(t)$ estimates passed the surrogate significance analysis for the two experimental conditions. Note that numbers consistently decrease in the CPT session, suggesting a higher inter-subject variability following a CPT than the resting state, and functional brain–heart interplay estimates related to EEG oscillations in the δ band were not retained for further analyses.

Aiming to verify whether the respiratory frequency lies within the HF band (0.15-0.4 Hz), we estimated the respiratory frequency for each experimental session, i.e., rest and CPT, by identifying the maximum of the signal frequency spectrum. Because of issues with the belt sensors during the recordings, 16 out of 24 respiratory signals were available for this analysis. Results indicate that the respiratory frequency was non-statistically different between the rest, 0.2056 ± 0.0389 Hz (median \pm median absolute deviation), and CPT, 0.2511 ± 0.0592 Hz (median \pm median absolute deviation), with a $p = 0.566$ from a Wilcoxon test for paired samples.

In Fig. 2, by comparing the first 30s of CPT w.r.t. the resting state, we observe that no significant changes are found in all the four EEG bands, thus meaning that brain-to-heart interplay during the first 30s of CPT elicitation is, on average, comparable to what measured in resting state. Between 30s and 60s after initiation of CPT, brain–heart interplay is much more significant in θ , β , and γ bands, and decreases w.r.t. the resting state. In the θ band, most of the anterior ventral scalp, and a portion of the dorsal parietal left lobe show a significant brain–heart interplay reduction. Both hemisphere show significant electrodes in the prefrontal and ventro-temporal regions, together with a ventro-central area. In the β band, significant alterations of brain–heart interplay occur, both on a central strip going from the prefrontal to the posterior parietal region, involving a widespread area in the ventro-central and prefrontal cortices, and on the right frontal lobe. brain–heart interplay alteration seems to be ubiquitous in the γ band in the time window that proceeds from 30s to 60s after the stimulus onset. Notably, the α frequency band does not highlight significant cluster in this time frame. In the third 30s window (60s-90s), few cluster of electrodes maintain their differences w.r.t. the resting state, particularly in the α , β , and γ bands, where single spots of deactivation are sustained. Considering the θ frequency range, instead, the midline prefrontal and ventro-central cortices continue being

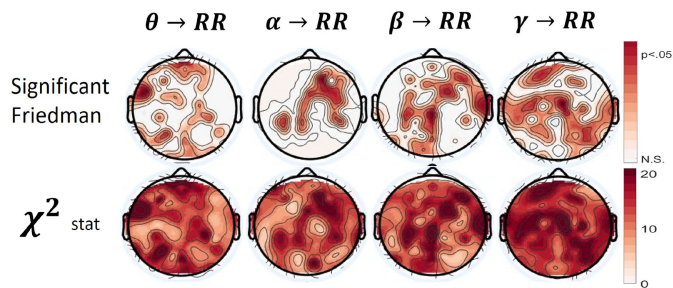


Fig. 3. Top row: The p-value topographic maps from the Friedman test for rest vs. CPT comparison on $I_{B \rightarrow H}$ for the following set: rest vs. CPT [0,30]s vs. CPT [30,60]s vs. CPT [60-90]s vs. CPT [90 120]s. Red color highlights statistical significance, whereas green color stands for not significant (N.S.) region. Bottom row: Topographical representation of χ^2 -square values obtained by the former Friedman test.

different in this time frame w.r.t. the resting state. In the last 30s (90s120s) of CPT stimulation, the brain–heart interplay reduction is highly significant, with some scalp regions being significant across all the four frequency bands, particularly the left dorso-parietal area. In the θ band, in the ventral semi-scalp brain–heart interplay from the frontal and left prefrontal areas, together with a restricted left central region are statistically significant. The α band, which was the less highlighted in the previous three time windows, shows now a broad significant area. Besides the left dorso-parietal cortex, which is in common with the other three frequency bands, in this case the ventral portion of the right hemisphere is strongly significant, together with a small portion of the right dorso-central cortex. The β frequency band depicts the dorso-left central and parietal regions, whereas the γ band report significant clusters also in the right counterpart and in a midline prefrontal area. The Z-values associated to the tests, which here have been thresholded to highlight significant regions can be found in the electronic supplementary material.

To highlight the difference in brain region activation through each session and time window, the Friedman test was applied on 2-minute of the resting state and all CPT session time windows. The results of the analysis are presented in Fig. 3. Here, brain–heart interplay variation occurs in all the four frequency bands considered. Specifically, in the θ band in the midline frontal cortex, in the left prefrontal and dorso central areas, whereas considering the α bands the right ventral hemisphere is highlighted. Statistical analysis in the β band highlights the strong difference in the anterior right lateral area and in a left posterior centro-parietal region; meanwhile, the γ band has a numerous set of significant electrodes across the whole scalp, except for the prefrontal right and occipital lobes.

In Fig. 4, results from the comparison between the resting state and the time-average across the whole CPT session using the Wilcoxon signed-rank test for paired data are shown. To obtain an overall insight on the difference between the two sessions, 2min of resting state was compared with 2min of CPT. This analysis indicates that brain–heart interplay is always significantly decreased in CPT w.r.t. the resting state in several

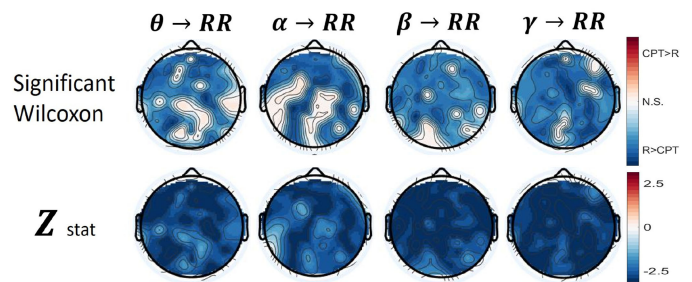


Fig. 4. The p-value topographic maps of $I_{B \rightarrow H}$ resulting from the Wilcoxon test comparing information transfer from the EEG to the heart-beat dynamics between the resting state and the whole CPT, by considering EEG bands. In the first row, red color highlights regions in which CPT has higher brain–heart interplay then rest, blue color mean the opposite, whereas green color stands for not significant (N.S.) regions. The second row depicts, for all bands, the Z-value associated to the Gaussian approximation of the former Wilcoxon test.

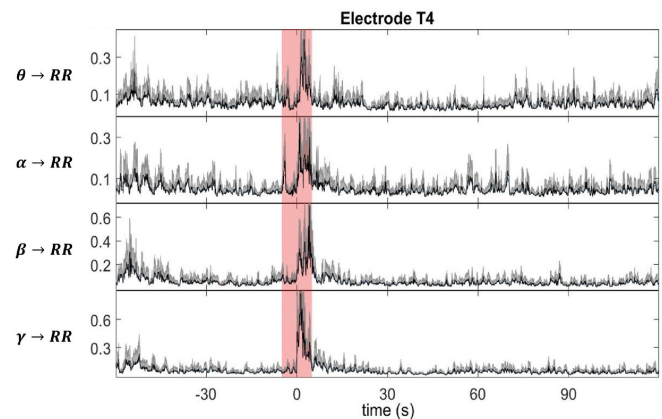


Fig. 5. The $I_{B \rightarrow H}$ plots (time-varying plots of brain–heart interplay) from the C4 electrode view. Continuous black line: estimation of the feature as median. Gray area: activity variation calculated by $MAD(X)$. Red area: highlighting transition time between resting state and CP. ($\theta \rightarrow RR$: the interplay considering the EEG θ band).

regions and frequency bands. The involved areas are the frontal and prefrontal cortices on both hemispheres in all the frequency ranges, the central regions (in the θ , β and γ bands), as well as the right temporal and dorso-parietal in all bands, and left temporal and centro-parietal areas for θ , β and γ bands.

We can track alterations in EEG–RR directional information exchange from the time course of $I_{B \rightarrow H}$ in Fig. 5. This feature indicates the variation of brain–heart interplay in specific frequency bands. To plot this time-varying behavior from an electrode viewpoint, we take the median value among all subjects. Group-wise variations are calculated by using the median absolute deviation (MAD), so that $MAD(X)$, where X is the vector of features, and are represented in the gray area. Here, we present time-varying plots from an exemplar electrode (i.e., T4) for all four significant frequency bands. The T4 electrode records activity from a region that has been found to be significant in many frequency bands, belonging to the right tempo-parietal lobe (see Fig. 4).

IV. DISCUSSION

Experimental results on a surrogate data analysis for the proposed estimates indicate a higher inter-subject variability in functional brain–heart interplay during a CPT elicitation than a resting state. We reported the results after the Wilcoxon and Friedman tests, and in the form of topographic maps of p-values, and depicted time-varying plots of brain–heart interplay in the form of the instantaneous point-process transfer entropy. Our experimental results on the functional information transfer from EEG to heartbeat dynamics are consistent with previous findings [1], [5], [39]. Specifically, our findings indicate that brain–heart interplay during the first 90s of the CPT is less affected by the α band activities, and we found that oscillations of this band are involved in brain–heart interplay at the end of the CPT, in which the sympathetic activity of the ANS is prominent. In addition, the results show that brain–heart interplay partially involves the frontal, prefrontal, central and parietal lobes (for all EEG frequency bands) in different time frames. The presence of frontal activities during the CPT is a new finding w.r.t. [39].

After CPT elicitation, there is a delay in the ANS activity of approximately 30s. This finding is similar to that obtained in [39] and references therein, where a neural response latency of approximately 27s for the low frequency component of the R-R intervals series is reported. This was consistent in all the frequency ranges considered. Next, the abrupt change of temperature caused an increase in sympathetic activity of the ANS, which is also characterized by an increase in blood pressure that later triggers the baroreflex mechanism (the mechanism is reported in terms of topographic maps in Fig. 2). To maintain the homeostatic condition of the body, parasympathetic activity is also increased after 30s of delay. One minute after CPT elicitation, the cortical involvement in regulation of the cardiovascular function is less prominent, which may indicate that the body has returned to its normal condition. From our results, we can argue that as the subject is very close to the pain threshold, after approximately 90s of holding a hand in the iced water, a significant sympathetic activity at the end of the CPT occurs. This significant change may indicate that at the end of the CPT, subjects may experience pain. In fact, it is known that pain perception is an inherent consequence of the test for most of the subjects [45], [67]–[69]. This phenomenon implies that the ANS activity tries to suppress pain in healthy subjects [70].

Comparing Fig. 3 with Fig. 4, we infer an overall brain–heart interplay variation after CPT stimulation. This outcome might imply suppression of brain activities for some period of CPT. Moreover, there is a good indication for the fact that the CAN activity is significant during the CPT because most of changes have been found in the central, prefrontal and parietal regions, which are closest to the CAN. This result is also enhanced from Figs. 2 and 4. The patterns of activity for the θ , β , and γ bands in Fig. 2, in the different 30sec time windows, are all enclosed to the corresponding brain–heart interplay patterns in Fig. 4 during considering the whole CPT session. A similar finding is also highlighted in the α band, between the brain–heart interplay pattern in Fig. 4 and in the last time window (90s–120s of CPT) in Fig. 2. Significant EEG patterns of activity for the frontal, prefrontal, and central lobes (premotor regions), and for

the θ , β , and γ bands in the ventro-parietal contralateral areas found to be significant here, have previously been assigned to motor inhibition, processing of mental stimuli, decision-making, control of unconscious and automatic reactions, motor planning, and pain perception [53]. The mentioned phenomena can be linked to CPT; that is, the subjects' patience in keeping their hands in the iced water, triggering autonomic activity (such as the baroreflex mechanism and pain perception), are parts of the CPT. The complexity of scalp response elicited by CPT stimulation explains our broad experimental findings, which are coherent with previous reports, and could merge what found at central and peripheral level. The proposed methodological framework comes with limitations. First, the model accounts for brain signals as modulating covariates of cardiovascular dynamics, neglecting other important autonomic covariates as the respiratory activity [71], directionality of cardiovascular control [72], blood pressure, and others. Second, the proposed implementation relies on a specific estimation procedure for the EEG spectrum and subsequent definition of EEG frequency bands, which may not be optimal for a functional brain–heart interplay study. In fact, while EEG aperiodic (1/f-like) components have putative physiological interpretations [73], the canonically defined frequency bands does not take them into account. Future studies shall investigate the sensitivity of brain–heart interplay estimates with respect to EEG and R-R intervals series (pre-)processing procedures.

While the standard definition/calculation of transfer entropy could be used to estimate the information transfer from the brain to the heartbeat, the use of inhomogeneous point-process comes with several advantages. Briefly, the use of point-process theory provides goodness of fit measures and quantitative methods and theorems to properly estimate the model parameters, including e.g. model order. Moreover, the inverse-Gaussian model takes into account underlying physiological dynamics of heartbeat generation. The model describes the first passage to threshold of the membrane voltages of the heart's pacemaker cells, while the model's autoregressive structure describes the dependence of the R-R interval lengths on the recent history of the autonomic inputs to the sino-atrial node, and the model's time-varying parameters capture the dynamic character of these sino-atrial node inputs [42]. The time-resolved estimation of functional brain–heart interplay might help with possible synchronization issues between the unevenly sampled heartbeat dynamics and evenly sampled EEG spectra, and overcomes the need for stationary inputs in standard transfer entropy estimation.

V. CONCLUSION

In this study, we demonstrated that the new probabilistic framework is effective for the quantitative characterization of functional brain–heart interplay. To our knowledge, this is the first attempt to quantify the directional information transfer from the brain to the heart in a time-resolved and probabilistic fashion. The proposed framework relies on multivariate, inhomogeneous point-process modeling of human heartbeat dynamics and the time-rescaling theorem, which enable users to have a probabilistic basis and to assess for the goodness-of-fit of the model. The statistical assessment of the estimated indices was accounted

comparing the extracted value to a null hypothesis of uncoupling through surrogates data analysis. For the model evaluation, we exploited a dataset that included heartbeat dynamics and EEG series of 24 subjects undergoing a CPT. Then, transfer entropy of the brain–heart system, $I_{B \rightarrow H}(t)$, which is defined in the continuous time, was calculated based on the estimated model parameters as a quantitative index for brain–heart interplay. The time-resolved transfer entropy enables the investigation of information transfer from the brain to the heart through sympathetic and parasympathetic activities of the ANS, whose branches innervate the cardiovascular system.

Future studies will be directed toward the use of model covariates related to brain dynamics other than EEG, for example, functional near-infrared spectroscopy and functional magnetic resonance imaging, as well as the application of the proposed framework to other datasets involving healthy subjects in different experimental conditions (e.g., emotional oscillation) and data from patients with mental disorders.

REFERENCES

- [1] F. Beissner *et al.*, “The autonomic brain: An activation likelihood estimation meta-analysis for central processing of autonomic function,” *J. Neurosci.*, vol. 33, no. 25, pp. 10 503–10511, 2013.
- [2] G. Valenza *et al.*, “The central autonomic network at rest: Uncovering functional MRI correlates of time-varying autonomic outflow,” *Neuroimage*, vol. 197, pp. 383–390, 2019.
- [3] M. Sklerov, E. Dayan, and N. Browner, “Functional neuroimaging of the central autonomic network: Recent developments and clinical implications,” *Clin. Auton. Res.*, vol. 29, no. 6, pp. 555–566, 2019.
- [4] G. Valenza *et al.*, “Uncovering complex central autonomic networks at rest: A functional magnetic resonance imaging study on complex cardiovascular oscillations,” *J. Roy. Soc. Interface*, vol. 17, no. 164, 2020, Art. no. 20190878.
- [5] A. Silvani *et al.*, “Brain–heart interactions: Physiology and clinical implications,” *Philos. Trans. Roy. Soc. A: Math., Phys. Eng. Sci.*, vol. 374, no. 2067, 2016, Art. no. 20150181.
- [6] M. Manea *et al.*, “Brain–heart axis–review article,” *J. Med. Life*, vol. 8, no. 3, 2015, Art. no. 266.
- [7] D. Hagemann, S. R. Waldstein, and J. F. Thayer, “Central and autonomic nervous system integration in emotion,” *Brain Cogn.*, vol. 52, no. 1, pp. 79–87, 2003.
- [8] V. H. Pereira *et al.*, “Stressed brain, diseased heart: A review on the pathophysiological mechanisms of neurocardiology,” *Int. J. Cardiol.*, vol. 166, no. 1, pp. 30–37, 2013.
- [9] S. Pyner, “The paraventricular nucleus and heart failure,” *Exp. Physiol.*, vol. 99, no. 2, pp. 332–339, 2014.
- [10] A. M. Dorrance and G. Fink, “Effects of stroke on the autonomic nervous system,” *Comprehensive Physiol.*, vol. 5, no. 3, pp. 1241–1263, 2011.
- [11] D. Hering, K. Lachowska, and M. Schlaich, “Role of the sympathetic nervous system in stress-mediated cardiovascular disease,” *Curr. Hypertension Rep.*, vol. 17, no. 10, pp. 1–9, 2015.
- [12] P. Taggart and P. Lambiase, “Anger, emotion, and arrhythmias: From brain to heart,” *Front. Physiol.*, vol. 2, p. 67, 2011.
- [13] Z. Chen *et al.*, “Brain–heart interaction: Cardiac complications after stroke,” *Circulation Res.*, vol. 121, no. 4, pp. 451–468, 2017.
- [14] M. Birket-Smith *et al.*, “Mental disorders and general well-being in cardiology outpatients–6-year survival,” *J. Psychosomatic Res.*, vol. 67, no. 1, pp. 5–10, 2009.
- [15] M. De Hert *et al.*, “Cardiovascular disease and diabetes in people with severe mental illness position statement from the european psychiatric association (epa), supported by the european association for the study of diabetes (easd) and the european society of cardiology (esc),” *Eur. Psychiatry*, vol. 24, no. 6, pp. 412–424, 2009.
- [16] M. M. Franks *et al.*, “Spouses’ provision of health-related support and control to patients participating in cardiac rehabilitation,” *J. Fam. Psychol.*, vol. 20, no. 2, 2006, Art. no. 311.
- [17] A. Craig, “Pain mechanisms: Labeled lines versus convergence in central processing,” *Annu. Rev. Neurosci.*, vol. 26, no. 1, pp. 1–30, 2003.
- [18] R. D. Lane *et al.*, “Neural correlates of heart rate variability during emotion,” *Neuroimage*, vol. 44, no. 1, pp. 213–222, 2009.
- [19] J. F. Thayer *et al.*, “A meta-analysis of heart rate variability and neuroimaging studies: Implications for heart rate variability as a marker of stress and health,” *Neurosci. Biobehav. Rev.*, vol. 36, no. 2, pp. 747–756, 2012.
- [20] G. Valenza *et al.*, “Assessment of spontaneous cardiovascular oscillations in parkinson’s disease,” *Biomed. Signal Process. Control*, vol. 26, pp. 80–89, 2016.
- [21] S. Rossi *et al.*, “The heart side of brain neuromodulation,” *Philos. Trans. Roy. Soc. A: Math., Phys. Eng. Sci.*, vol. 374, no. 2067, 2016, Art. no. 20150187.
- [22] F. Corrigan, J. Fisher, and D. Nutt, “Autonomic dysregulation and the window of tolerance model of the effects of complex emotional trauma,” *J. Psychopharmacol.*, vol. 25, no. 1, pp. 17–25, 2011.
- [23] A. R. Damasio *et al.*, “Subcortical and cortical brain activity during the feeling of self-generated emotions,” *Nature Neurosci.*, vol. 3, no. 10, pp. 1049–1056, 2000.
- [24] X.-l. *et al.*, “Attenuated or absent hrv response to postural change in subjects with primary insomnia,” *Physiol. Behav.*, vol. 140, pp. 127–131, 2015.
- [25] B. Silvioli *et al.*, “Autonomic nervous system dysregulation in irritable bowel syndrome,” *Neurogastroenterol. Motility*, vol. 27, no. 3, pp. 423–430, 2015.
- [26] S. J. Leistedt *et al.*, “Decreased neuroautonomic complexity in men during an acute major depressive episode: Analysis of heart rate dynamics,” *Transl. Psychiatry*, vol. 1, no. 7, pp. e 27–e27, 2011.
- [27] G. Valenza *et al.*, “Complexity variability assessment of nonlinear time-varying cardiovascular control,” *Sci. Rep.*, vol. 7, no. 1, pp. 1–15, 2017.
- [28] B. W. Penninx *et al.*, “Understanding the somatic consequences of depression: Biological mechanisms and the role of depression symptom profile,” *BMC Med.*, vol. 11, no. 1, 2013, Art. no. 129.
- [29] R. Schandry, B. Sparrer, and R. Weitkunat, “From the heart to the brain: A study of heartbeat contingent scalp potentials,” *Int. J. Neurosci.*, vol. 30, no. 4, pp. 261–275, 1986.
- [30] V. Catrambone *et al.*, “Functional brain–heart interplay extends to the multifractal domain,” *Philos. Trans. Roy. Soc. A: Math., Phys. Eng. Sci.*, 2021.
- [31] G. Valenza *et al.*, “Combining electroencephalographic activity and instantaneous heart rate for assessing brain–heart dynamics during visual emotional elicitation in healthy subjects,” *Philos. Trans. Roy. Soc. A: Math., Phys. Eng. Sci.*, vol. 374, no. 2067, 2016, Art. no. 20150176.
- [32] V. Catrambone *et al.*, “Functional linear and nonlinear brain–heart interplay during emotional video elicitation: A maximum information coefficient study,” *Entropy*, vol. 21, no. 9, 2019, Art. no. 892.
- [33] L. Faes *et al.*, “Linear and non-linear brain–heart and brain–brain interactions during sleep,” *Physiol. Meas.*, vol. 36, no. 4, 2015, Art. no. 683.
- [34] K. Schiecke *et al.*, “Brain–heart interactions considering complex physiological data: Processing schemes for time-variant, frequency-dependent, topographical and statistical examination of directed interactions by convergent cross mapping,” *Physiol. Meas.*, vol. 40, no. 11, 2019, Art. no. 114001.
- [35] S. Schulz *et al.*, “Altered causal coupling pathways within the central–autonomic–network in patients suffering from schizophrenia,” *Entropy*, vol. 21, no. 8, 2019, Art. no. 733.
- [36] A. Bashan *et al.*, “Network physiology reveals relations between network topology and physiological function,” *Nat. Commun.*, vol. 3, no. 1, pp. 1–9, 2012.
- [37] L. Faes *et al.*, “Estimating the decomposition of predictive information in multivariate systems,” *Phys. Rev. E*, vol. 91, no. 3, 2015, Art. no. 0 32904.
- [38] A. Greco *et al.*, “Lateralization of directional brain–heart information transfer during visual emotional elicitation,” *Amer. J. Physiol.-Regulatory, Integrative Comp. Physiol.*, vol. 317, no. 1, pp. R 25–R38, 2019.
- [39] V. Catrambone *et al.*, “Time-resolved directional brain–heart interplay measurement through synthetic data generation models,” *Ann. Biomed. Eng.*, vol. 47, no. 6, pp. 1479–1489, 2019.
- [40] A. Talebi, “An inhomogeneous point-process model for the assessment of the brain-to-heart functional interplay: A pilot study,” in *Proc. IEEE 42nd Annu. Int. Conf. Eng. Med. Biol. Soc.*, 2020, pp. 557–560.
- [41] U. R. Acharya *et al.*, “Heart rate variability: A review,” *Med. Biol. Eng. Comput.*, vol. 44, no. 12, pp. 1031–1051, 2006.
- [42] R. Barbieri *et al.*, “A point-process model of human heartbeat intervals: New definitions of heart rate and heart rate variability,” *Amer. J. Physiol.-Heart Circulatory Physiol.*, vol. 288, no. 1, pp. H 424–H435, 2005.
- [43] E. N. Brown *et al.*, “The time-rescaling theorem and its application to neural spike train data analysis,” *Neural Comput.*, vol. 14, no. 2, pp. 325–346, 2002.

- [44] D. U. Silverthorn and J. Michael, "Cold stress and the cold pressor test," *Adv. Physiol. Edu.*, vol. 37, no. 1, pp. 93–96, 2013.
- [45] J. Cui, T. E. Wilson, and C. G. Crandall, "Baroreflex modulation of muscle sympathetic nerve activity during cold pressor test in humans," *Amer. J. Physiol.-Heart Circulatory Physiol.*, vol. 282, no. 5, pp. H 1717–H1723, 2002.
- [46] M. D. Esler, "Mental stress, panic disorder and the heart," *Stress Med.*, vol. 14, no. 4, pp. 237–243, 1998.
- [47] W. Lovallo, "The cold pressor test and autonomic function: A review and integration," *Psychophysiol.*, vol. 12, no. 3, pp. 268–282, 1975.
- [48] R.-C. Peng *et al.*, "Time-frequency analysis of heart rate variability during the cold pressor test using a time-varying autoregressive model," *Physiol. Meas.*, vol. 36, no. 3, 2015, Art. no. 441.
- [49] V. Catrambone *et al.*, "Heartbeat dynamics analysis under cold-pressure test using wavelet p-leader non-gaussian multiscale expansions," in *Proc. 41st Annu. Int. Conf. IEEE Eng. Med. Biol. Soc.*, 2019, pp. 2023–2026.
- [50] P. F. Chang, L. Arendt-Nielsen, and A. C. Chen, "Dynamic changes and spatial correlation of eeg activities during cold pressor test in man," *Brain Res. Bull.*, vol. 57, no. 5, pp. 667–675, 2002.
- [51] S. Ferracuti *et al.*, "Quantitative eeg modifications during the cold water pressor test: Hemispheric and hand differences," *Int. J. Psychophysiol.*, vol. 17, no. 3, pp. 261–268, 1994.
- [52] V. Catrambone *et al.*, "Wavelet p-leader non-Gaussian multiscale expansions for EEG series: An exploratory study on cold-pressor test," in *Proc. 41st Annu. Int. Conf. IEEE Eng. Med. Biol. Soc.*, 2019, pp. 7096–7099.
- [53] R. C. Coghill *et al.*, "Pain intensity processing within the human brain: A bilateral, distributed mechanism," *J. Neurophysiol.*, vol. 82, no. 4, pp. 1934–1943, 1999.
- [54] R. M. Harper *et al.*, "Fmri responses to cold pressor challenges in control and obstructive sleep apnea subjects," *J. Appl. Physiol.*, vol. 94, no. 4, pp. 1583–1595, 2003.
- [55] S. O. Elias and R. E. Ajayi, "Effect of sympathetic autonomic stress from the cold pressor test on left ventricular function in young healthy adults," *Physiol. Rep.*, vol. 7, no. 2, 2019, Paper e 13985.
- [56] M. C. Hendriks-Balk *et al.*, "Brainstem correlates of a cold pressor test measured by ultra-high field fmri," *Front. Neurosci.*, vol. 14, p. 39, 2020.
- [57] V. Napadow, R. Sclocco, and L. A. Henderson, "Brainstem neuroimaging of nociception and pain circuitries," *Pain Rep.*, vol. 4, no. 4, 2019.
- [58] R. Sclocco *et al.*, "Challenges and opportunities for brainstem neuroimaging with ultrahigh field mri," *Neuroimage*, vol. 168, pp. 412–426, 2018.
- [59] G. B. Stanley, K. Poolla, and R. A. Siegel, "Threshold modeling of autonomic control of heart rate variability," *IEEE Trans. Biomed. Eng.*, vol. 47, no. 9, pp. 1147–1153, Sep. 2000.
- [60] G. Valenza *et al.*, "Instantaneous transfer entropy for the study of cardiovascular and cardiorespiratory nonstationary dynamics," *IEEE Trans. Biomed. Eng.*, vol. 65, no. 5, pp. 1077–1085, May 2018.
- [61] T. Schreiber, "Measuring information transfer," *Phys. Rev. Lett.*, vol. 85, pp. 461–464, Jul. 2000. [Online]. Available: <https://link.aps.org/doi/10.1103/PhysRevLett.85.461>
- [62] J. Pan and W. J. Tompkins, "A real-time QRS detection algorithm," *IEEE Trans. Biomed. Eng.*, vol. BME-32, no. 3, pp. 230–236, Mar. 1985.
- [63] L. Citi, E. N. Brown, and R. Barbieri, "A real-time automated point-process method for the detection and correction of erroneous and ectopic heartbeats," *IEEE Trans. Biomed. Eng.*, vol. 59, no. 10, pp. 2828–2837, Oct. 2012.
- [64] A. Delorme and S. Makeig, "Eeglab: An open source toolbox for analysis of single-trial eeg dynamics including independent component analysis," *J. Neurosci. Methods*, vol. 134, no. 1, pp. 9–21, 2004.
- [65] L. J. Gabard-Durnam *et al.*, "The harvard automated processing pipeline for electroencephalography (happe): Standardized processing software for developmental and high-artifact data," *Front. Neurosci.*, vol. 12, p. 97, 2018.
- [66] A. Porta and L. Faes, "Wiener-granger causality in network physiology with applications to cardiovascular control and neuroscience," *Proc. IEEE Proc. IRE*, vol. 104, no. 2, pp. 282–309, Feb. 2016.
- [67] B. Hellström and U. Lundberg, "Pain perception to the cold pressor test during the menstrual cycle in relation to estrogen levels and a comparison with men," *Integrative Physiol. Behav. Sci.*, vol. 35, no. 2, pp. 132–141, 2000.
- [68] E. R. Hilgard, A. H. Morgan, and H. Macdonald, "Pain and dissociation in the cold pressor test: A study of hypnotic analgesia with" hidden reports" through automatic key pressing and automatic talking," *J. Abnorm. Psychol.*, vol. 84, no. 3, 1975, Art. no. 280.
- [69] M. E. Geisser, M. E. Robinson, and W. E. Pickren, "Differences in cognitive coping strategies among pain-sensitive and pain-tolerant individuals on the cold-pressor test," *Behav. Ther.*, vol. 23, no. 1, pp. 31–41, 1992.
- [70] T. Schlereth and F. Birklein, "The sympathetic nervous system and pain," *Neuromol. Med.*, vol. 10, no. 3, pp. 141–147, 2008.
- [71] L. J. Badra *et al.*, "Respiratory modulation of human autonomic rhythms," *Amer. J. Physiol.-Heart Circulatory Physiol.*, vol. 280, no. 6, pp. H 2674–H2688, 2001.
- [72] A. Porta *et al.*, "Accounting for respiration is necessary to reliably infer granger causality from cardiovascular variability series," *IEEE Trans. Biomed. Eng.*, vol. 59, no. 3, pp. 832–841, Mar. 2012.
- [73] T. Donoghue *et al.*, "Parameterizing neural power spectra into periodic and aperiodic components," *Nature Neurosci.*, vol. 23, no. 12, pp. 1655–1665, 2020.